AAS 14-324

ANALYTICAL MODEL FOR THE PROPAGATION OF SMALL DEBRIS OBJECTS AFTER A FRAGMENTATION EVENT

Francesca Letizia[*], Camilla Colombo[†], and Hugh G. Lewis[‡]

Current debris evolutionary models usually neglect fragments smaller than 10 cm in their predictions because of the high computational effort they add to the simulation. However, also small fragments can be dangerous to operational satellites. This work proposes an analytical approach to describe the evolution of a cloud of small fragments generated by a collision in Low Earth Orbit. The proposed approach considers the cloud globally and derives analytically its evolution in terms of density, under the effect of drag. As a result, the analytical approach allows the representation of small fragments and noticeably reduces the computational time.

INTRODUCTION

Past space missions left in orbit a large number of non operational objects, whose size varies from large rocket stages to sub-millimetre-size fragments. Radars are able to track objects larger than 10 cm in Low Earth Orbit (LEO) and then collision avoidance manoeuvres can be implemented. Small objects, on the other hand, are not trackable, so shields are adopted on spacecraft to protect them from impacts. However, shields are effective only for fragments smaller than 1 cm.[1] As a result, a large population of space debris is too big for shields but too small to be tracked and poses a risk to operational spacecraft[2] as it may cause for spacecraft anomalies[3] or even more serious damage to satellites.[4]

Therefore, it is important to characterise fragments, in particular their motion in orbit. Some research on debris long-term evolution was conducted for the debris population down to 1 cm[5,6] and 5 cm,[7] but most of recent studies neglect objects smaller than 10 cm because their number is so large that the simulation of the debris environment would be extremely expensive in terms of computational time and because the focus has been on the most dangerous impactors.[4] However, this partial representation of space debris environment may result in an underestimation of the collision risk for operational satellites. For this reason, an increasing effort is currently underway to update debris studies by including small objects and to formulate simplified models able to provide quick estimations of space debris evolution.[8]

Some debris models (e.g. SDM, DAMAGE, DELTA) are able to deal with small fragments grouping them into representative objects, from whose propagation it is possible to re-build the evolution of small objects. For example, an effective technique to reduce the computational time is the method proposed by Rossi et al.[9] where the fragment propagation is simplified in three ways:

[*]PhD candidate, Astronautics Research Group, University of Southampton, UK, SO17 1BJ, f.letizia@soton.ac.uk
[†]Lecturer, PhD, Astronautics Research Group, University of Southampton, SO17 1BJ, UK, currently Marie Curie Research fellow at Politecnico di Milano, Italy, camilla.coliombo@polimi.it
[‡]Senior lecturer, PhD,, Astronautics Research Group, University of Southampton, UK, SO17 1BJ, h.g.lewis@soton.ac.uk

- only the most relevant perturbation, drag, is considered to study the fragment motion in LEO,
- the dynamics considered makes use of analytical expressions obtained by King-Hele[10] to describe the secular effect of aerodynamic drag,
- only some representative objects are propagated.

The debris population is divided into bins in altitude and object size and only one object per bin is propagated. The result of the propagation is used to estimate how fragments move among the bins; from this, together with the launch frequency and explosion and collision rates for each bin, the evolution of the object number per bin is obtained. In this way, a cloud of more than 800 objects is propagated for 100 years in less than 10 s.[11]

Kebschull et al.[12,13] have further developed and improved this approach, considering also active debris removal, dividing debris objects into eccentricity bins and distinguishing between intact objects and fragments. Moreover, the parameters in the evolution equations were obtained through a fitting process of the full numerical model LUCA; in this way, the output of the simplified model is coherent with the full numerical one, but the simulation time is strongly reduced.

Similarly, Lewis et al.[14] used the data generated by the numerical model DAMAGE to build the simplified model CONCEPT, which is able to study the consequences of a single collision event. Although the current implementation considers only objects larger than 10 cm, its approach can be extended to smaller fragments. The background debris population is built from DAMAGE data and stored in bins of altitude, right ascension and declination: for each bin the distribution of relevant quantities (e.g. spatial density, collision probability, object type, mass, area, orbital parameters) is stored. CONCEPT is then able to estimate candidates for collision and the most likely parameters (i.e. mass, energy) for the fragmentation event. Here, DAMAGE is used again to generate the debris cloud and to propagate the fragments; at each time step the distributions stored in the bins are updated with the contribution from the new cloud, so that it is possible to assess the impact of the simulated event on the global population. This method requires five minutes to propagate a typical scenario for 200 years.

These two last examples rely on several runs of a full model, whose output is then stored and used by the simplified model. This implies that if part of the full model changes (for example, the breakup model), it should be run again to obtain updated parameters.

The present work proposes and evaluates the accuracy of a method that instead of integrating the fragment trajectories, studies globally the fragment cloud formed after a collision. In particular, the cloud density is the state variable of the method and its evolution is obtained analytically, following the approach proposed by McInnes[15] and used also to describe the motion of interplanetary dust,[16] high area-to-mass ratio spacecraft[17] and nano-satellite constellations.[18]

Purely analytical models are not common for long-term debris modelling and usually they are used for Geosynchronous Earth Orbit (GEO) objects, where drag is negligible and it is possible to introduce an Hamiltonian formulation for the forces acting on the fragments.[19,20]

However, LEO is the most crucial region for space debris, because of the higher object density and higher collision velocities compared to GEO;[21,22] an analytical model applicable in LEO and able to follow small fragment motion can be a useful extension of existing models to increase the accuracy in the prediction of the collision risk for operational spacecraft.

ANALYTICAL APPROACH

The algorithm behind the proposed analytical debris model can be represented as in the block diagram in Figure 1, where four main building blocks are presented:

- a break up model that generates the fragment properties (i.e. number, mass, area, speed) given the energy of the collision;
- a numerical propagator to describe the evolution with time of the fragment orbital parameters until the analytical propagation becomes applicable;
- a method to translate the information on the orbital parameters of each single fragments into a continuous density function, useful to compute the collision risk associated with the cloud;
- an analytical propagator to describe the evolution with time of the cloud spatial density on the long term.

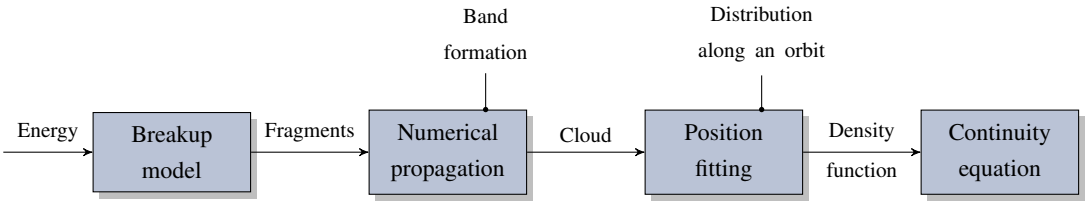

Figure 1: Algorithm building blocks.

Breakup model

The model here adopted is the NASA breakup model.[23,24] It was implemented considering non-catastrophic collisions and only for fragments with size in the range 1 mm-8 cm, to avoid the discontinuities present in the model and to study how the distributions present in the NASA breakup model influence the fragment dispersion. The choice of studying non-catastrophic collisions is also driven by the recent observations that most of the recorded past collisions were non-catastrophic ones.[25]

The number of fragments N_f larger than a characteristic length L_c produced by a collision is given by

$$N_f(L_c) = 0.1(M_e)^{0.75}(L_c)^{(-1.71)}; \tag{1}$$

where M_e is the reference mass of the collision. For M_e, Johnson and Krisko[23] indicate

$$M_e[\text{kg}] = M_p[\text{kg}]v_c[\text{km/s}] \tag{2}$$

where M_p is the projectile mass and v_c the collision velocity. The expression was then corrected by Krisko[24] as

$$M_e[\text{kg}] = M_p[\text{kg}](v_c[\text{km/s}])^2 \tag{3}$$

and this last version is here used.* The NASA breakup model provides also the distributions of area-to-mass ratio and velocity variation respectively as function of the characteristic length and the

*Krisko, Paula (2013), personal correspondence of June 10th, Sr. Scientist Specialist, Orbital Debris Modeling Lead, JSC/JETS/Jacobs Tech

area-to-mass ratio. In this work a maximum ejection velocity is introduced, equal to $1.3\,v_c$ and the ejection velocity direction is randomised.

The limits of the NASA breakup model, especially in the sub-centimetre range, are known: it is based on a limited database, so it is not clear how representative the model is.[26] For this reason, some studies are ongoing to improve the model, adding more data points or introducing some physical equation (e.g. the momentum conservation).[26,27,28] However, at the moment no better breakup model is available and the NASA model can be considered as a standard as it is the most used in space debris models[29] (LEGEND, MASTER, DAMAGE). Moreover, the analytical method proposed here does not rely on a specific breakup model: when an alternative model becomes available, only the first block shown in Figure 1 will be changed and the other blocks will not require any modification.

Numerical propagation

Immediately after the collision, the fragments form a dense cloud concentrated in the location where the breakup occurred (Figure 2a): as each fragment has a slightly different energy, the cloud is stretched along the orbit of the parent spacecraft. In addition, the Earth's oblateness causes a variation of the argument of periapsis ω (Figure 2b) and of the longitude of the ascending node Ω, so that the cloud is finally spread into a band around the Earth (Figure 2c). As a result, ω, Ω and the true anomaly ν are randomised, usually after few months; starting from this point drag can be considered as the dominant perturbation.[30] The analytical method, which represents only the drag effect, can be applied only from this moment, while numerical propagation is required to follow the first phases of the cloud evolution.

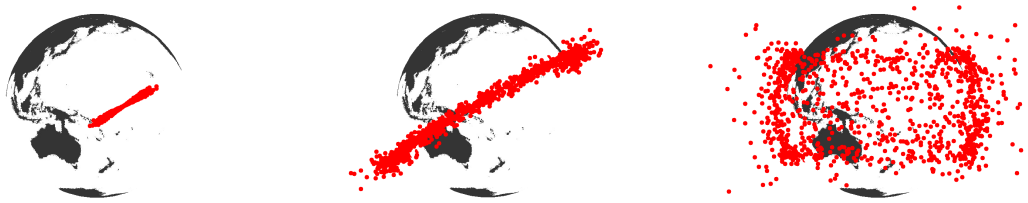

(a) Ellipsoid (b) Toroid (c) Band

Figure 2: Phases of debris cloud evolution as classified by Jehn.[30]

The fragment orbital parameters are propagated numerically using Gauss' equations:[31] for the Earth's oblateness, only J_2 is considered as the transition to the band occurs in a short time. The drag effect is computed through King-Hele's expressions[10] for eccentricity e lower than 0.2; no atmospheric rotation is considered; the maximum altitude below which drag is considered is $1000\,\text{km}$ and the propagation is stopped if the fragment perigee altitude is below $50\,\text{km}$. For the atmospheric density ρ, an exponential model is used

$$\rho = \rho_{\text{ref}} \exp\left(- \frac{h - h_{\text{ref}}}{H} \right) \tag{4}$$

where h is the altitude, h_{ref} is the reference altitude where the reference density ρ_{ref} and the scale height H are defined. The reference values $h_{\text{ref}}, \rho_{\text{ref}}, H$ and are taken from Vallado[31] and h_{ref} is set

as the altitude where the collision occurs and its value is kept constant for the whole simulation*.

The numerical propagation ends when the band is formed: this can be verified numerically comparing the distribution of the angles (ν, ω, Ω) with a uniform distribution between $-\pi$ and π through the Kolmogorov-Smirnov test.[32] Another approach, which is the one used for the results shown in the following, is to use one of the analytical expressions present in literature[33,34,35] to estimate the time required for the band formation. In particular, Ashenberg[35] estimated the time for band formation T_b as the maximum between the time of the dispersion of the longitude of the ascending node Ω (T_Ω) and the one of the argument of periapsis ω (T_ω). They are expressed as

$$\begin{aligned} T_b &= \max(T_\Omega, T_\omega) \\ T_\Omega &= \frac{\pi}{3J_2 \frac{R_E^2}{a^3}(7\cos i \cos\beta_\Omega + \sin i \cos u \sin\beta_\Omega)\delta v} \\ T_\omega &= \frac{\pi}{3J_2 \frac{R_E^2}{a^3}(7(2-\frac{5}{2}\sin^2 i)\cos\beta_\omega + \frac{5}{2}\sin 2i \cos u \sin\beta_\omega)\delta v} \end{aligned} \tag{5}$$

where

$$\begin{aligned} \tan\beta_\Omega &= \frac{1}{7}\tan i \cos u \\ \tan\beta_\omega &= \frac{5\sin 2i \cos u}{14(2-\frac{5}{2}\sin^2 i)} \end{aligned} \tag{6}$$

and R_E is the Earth's radius; a, i, u are respectively the semi-major axis, the inclination and the longitude of the periapsis of the orbit where the fragmentation occurs; δv is the (average) variation of the velocity due to the fragmentation event. The accuracy of these analytical expressions, compared to the numerical estimation, was verified in a previous work.[36]

Position fitting

Once the band is formed, the information on the fragment positions is translated into a continuous density function that will be the initial condition for the analytical method. In the previous version of the model,[36] the density function was built from the distribution of fragments in distance from the Earth r or semi-major axis a, whereas here it is built on the probability of intercepting fragments at a certain altitude. This figure is, in fact, the most important if the method is used to compute the impact of the cloud on the collision risk for operational satellites and, as explained in the following section, only one coordinate is considered.

The probability density for a cloud is built starting from the expression by McInnes and Colombo[37] describing the number density of objects along one orbit,

$$n_{\nu,i}(\nu) = \frac{(1+e_i)^2}{(1+e_i\cos\nu)^2}, \tag{7}$$

where the density expression is selected such that $n_{\nu,i}(\nu = 0) = 1$. Equation 7 expresses the condition that, as an object is slower close to the apogee, it spends more time in that region of space

*These settings are used also for the fully numerical simulation of the cloud evolution used to validate the analytical approach. The approximation of constant h_{ref}, ρ_{ref}, H can be relaxed; here it is kept for simplicity as the aim of the work is to validate the analytical propagation compared to the numerical one.

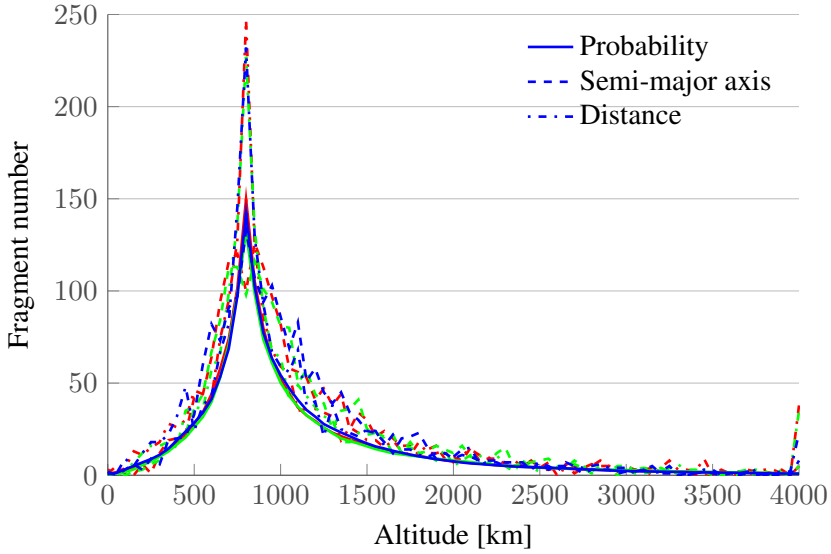

Figure 3: Comparison among three different distributions that may be used to describe the initial condition: solid line refers to the probability density as defined in Equation 8, dashed line to the semi-major axis distribution, dash-dot line to distance distribution. Each colour refers to a different run of the break-up model.

and so there is higher probability of interception. Equation 7 can be easily expressed in terms of the distance from the Earth r as

$$n_i(r) = \frac{3}{2} \frac{r^2}{a_i^3(3e_i + e_i^3)}, \tag{8}$$

where the density is rescaled so that the integral of the expression in Equation 8 between the perigee and the apogee radius is equal to 1. In this way, it is possible to sum the contribution from each fragment to obtain the probability density for the whole cloud $n = \sum_i n_i$ (Figure 3).

Besides the connection with collision risk computation, this approach presents also an additional advantage: the initial condition built in terms of probability density is much less dependent on the single run of the break up model compared to the one built on the semi-major axis or on the distance. The break-up model contains in itself some random values (e.g. to define the fragment distribution in terms of ejection velocity) and so more runs are required to generate data with statistical meaning. Figure 3 presents the comparison among possible initial conditions; three different runs of the break-up model are presented, each one plotted in a different colour. It is possible to see that, in contrast to the simple distribution in r (dash-dot line), the probability density (solid line) has only a limited variation with the specific analysed run; moreover, the distribution in r tends to the probability density if many cases are run and analysed together.

Analytical propagation

Once the initial fragment density is defined, the continuity equation is used to derive analytically the density evolution with time under the drag effect, following the approach developed by McInnes[18] and here summarised briefly.

Neglecting discontinuous events (sources, for example launches, and sinks, for example active

debris removal), the continuity equation can be written as

$$\frac{\partial n}{\partial t} + \nabla \bullet \mathbf{f} = 0; \tag{9}$$

where n is the fragment density and the term $\mathbf{f}$ is the vector field that causes the fragment position to vary with time t.

The distance r is the only considered coordinate, so a spherical symmetry is assumed; as stated before, this assumption and modelling only drag effect imply that the analytical propagation becomes applicable after the cloud has formed a band around the Earth. The vector field has then only one component in the radial direction and it is written as

$$f_r = v_r n(r,t). \tag{10}$$

The drift velocity in the radial direction v_r is obtained from the expression of drag acceleration

$$a_D = \frac{1}{2}\frac{C_D A}{M}\rho(r)v^2 \tag{11}$$

where C_D is the drag coefficient of the fragment, which is assumed to be constant and equal to 2.2;[31] A is the fragment cross-sectional area; M is the fragment mass; v is the fragment velocity and $\rho(r)$ is the atmosphere density, which depends on the distance from the Earth and is expressed through the exponential model in Equation 4. Introducing, from McInnes,[18] the parameter ε,

$$\varepsilon = \sqrt{\mu}\frac{C_D A}{M}\rho_{\text{ref}} \exp\Big(\frac{h_{\text{ref}}}{H}\Big), \tag{12}$$

which collects all the terms that do not depend on r, and assuming that the fragment orbits are circular, the final expression for v_r is obtained

$$v_r = -\varepsilon\sqrt{r}\exp\Big(-\frac{r}{H}\Big). \tag{13}$$

Introducing the approximation

$$\sqrt{r} \approx \sqrt{R_H}, \qquad R_H = R_E + h_{\text{ref}}, \tag{14}$$

where R_E is the Earth's radius and h_{ref} is the altitude where the initial collision occurs as in Equation 4, and applying the method of characteristics, McInnes[18] obtained an explicit expression for the density evolution,

$$\begin{aligned}\log\{n(r,t)\} = \log\{-\varepsilon r^{5/2}\exp[-r/H]\}^{-1} + \\ + \Psi\{\exp[r/H] + (\varepsilon\sqrt{R_H}/H)t\}\end{aligned} \tag{15}$$

where the function Ψ is obtained from the initial condition $n(r, t = 0)$ and the characteristics z at $t = 0$

$$\Psi(z) = \log\{n(r(z),0)\} - \log\{r(z)^2 v_r(z)\}^{-1}. \tag{16}$$

Equation 15 provides a fully analytical expression to compute the effect of drag on the cloud and the analytical propagation always acts on the cloud globally, not on the single fragments. Therefore, in this case, the model is *analytical* in the sense that, once the initial density is known, the cloud

density at any time is immediately known, without any numerical integration of the fragment trajectories, differently from previous models.[9,12,14] Moreover, Equation 16 shows that no particular operation is needed on the function $n(r, 0)$, providing large flexibility on the functions that can be used to describe the initial condition. This means that the initial condition can be built easily starting from different kind of fragmentation phenomena.

The parameter ε, defined in Equation 12, is not constant for the whole cloud as the fragments have different area-to-mass ratios, A/M. To improve the accuracy of the model, N bins in area-to-mass ratio are defined. For each bin, an average ε_i is assumed and the corresponding density n_i is obtained according to Equation 15; all the partial densities n_i are summed to obtain the global cloud density n.

COMPARISON WITH NUMERICAL PROPAGATION

The results here refer to a fragmentation generated by the non-catastrophic collision between a spacecraft and a projectile of $100\,\mathrm{g}$ with a collision velocity of $1\,\mathrm{km\,s^{-1}}$. The parent orbit of the spacecraft is planar and circular, with altitude equal to $800\,\mathrm{km}$.The collision generates 2397 fragments, whose area-to-mass ratios range from 0.0298 to $15.4\,\mathrm{m^2\,kg^{-1}}$ in the specific considered run of the breakup model. In fact, all the following results refer to this single run of the NASA break-up model as the study aims to compare and validate the analytical propagation against the numerical propagation.

The fragments generated by the breakup model are divided into 10 A/M bins, each one containing the same number of objects. Other definitions of the bins are possible (as for example logarithmically spaced intervals) but the result in terms of global density of the cloud is almost identical.

The band is formed after almost 64 days and then the analytical propagation is applied. Figure 4 shows the cloud density, obtained with the analytical method, at the band formation (Figure 4a), and 1000 days later (Figure 4b). At the band formation, the Figure 4a indicates a distinct peak

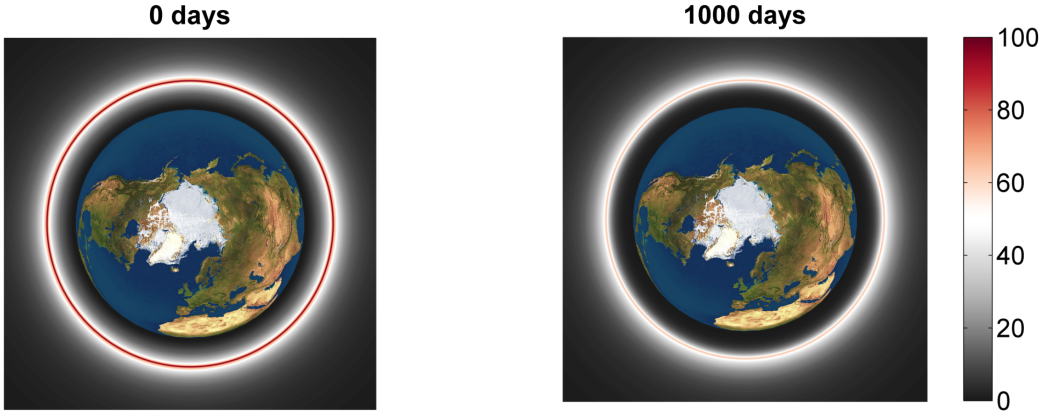

(a) (b)

Figure 4: Visualisation of cloud density at (a) the band formation and (b) after 1000 days. The density $n(r, t)$ is expressed in number of fragments in a spherical shell of radius r. The plot is not in scale.

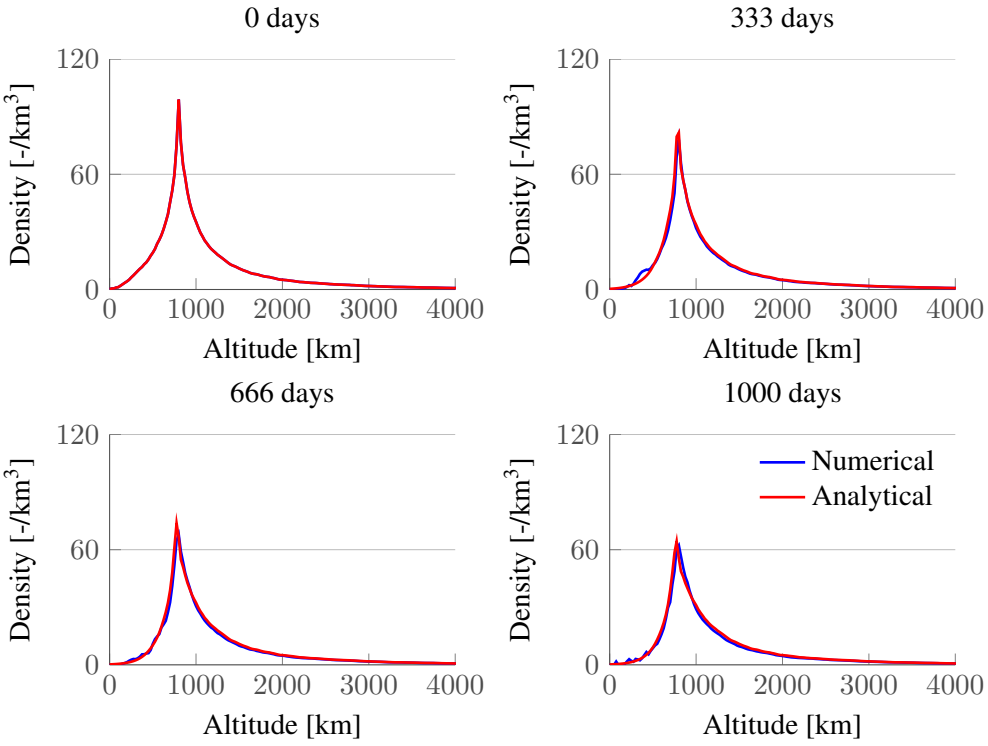

Figure 5: Evolution of the cloud density as a function of time after the band formation, for a fragmentation at 800 km.

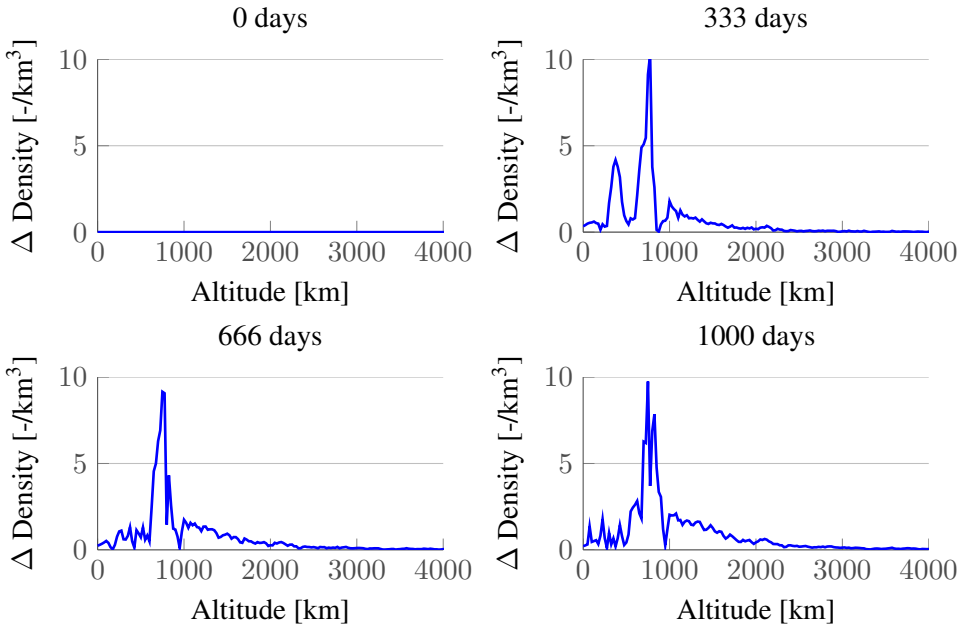

Figure 6: Absolute error in the cloud density as a function of time after the band formation, for a fragmentation at 800 km.

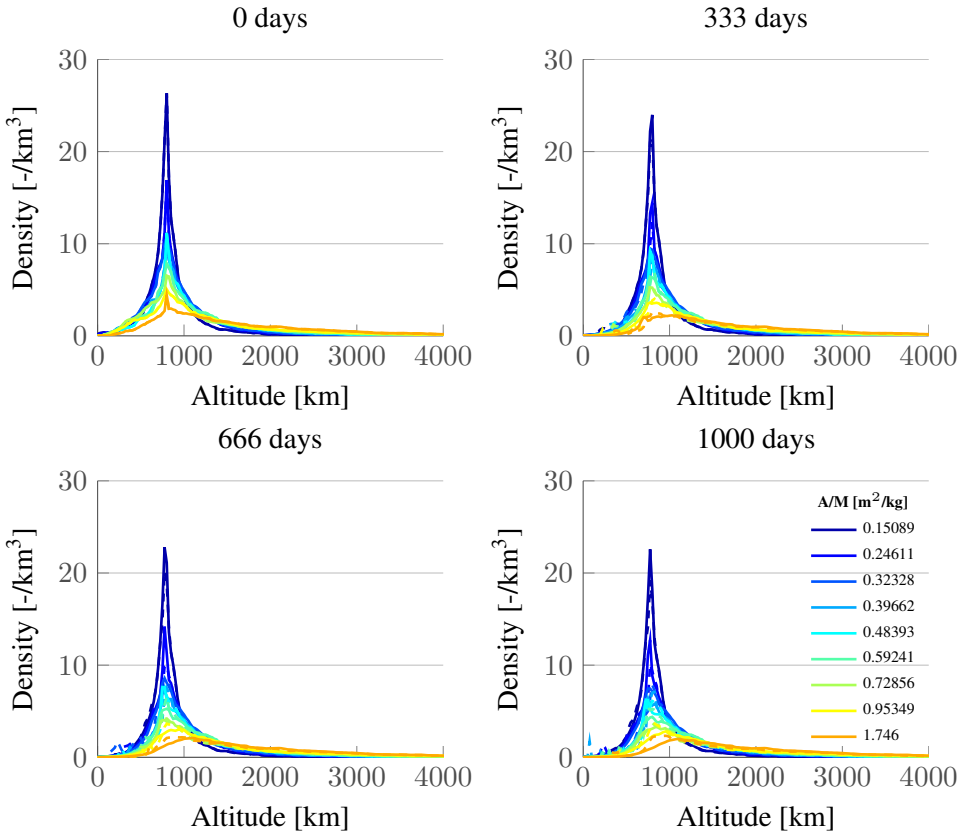

Figure 7: Evolution of the cloud density as a function of time after the band formation, for a fragmentation at 800 km. The colours refer to different values of the area-to-mass ratio; dashed lines indicate the result of the numerical propagation, solid lines the analytical one. Each bin contains the same number of fragments.

(the red circle) in the cloud density at the altitude of the breakup. After 1000 days (Figure 4b) drag has reduced the peak and also the number of fragments at low altitudes as the area below the fragmentation altitude is almost completely black; the density at high altitude is, instead, almost unchanged.

More in detail, Figure 5 shows the comparison between the numerical (in blue) and the analytical (in red) propagation of the cloud probability density. The absolute error between the two curves is shown in Figure 6: the maximum error occurs between 750 and 800 km where, locally, the relative error reaches the value of 0.2. Globally, the analytical method is able to follow the cloud evolution very well, catching both the reduction of the fragment number and the different effect of drag on low and high altitude.

Figure 7 shows in detail the propagation of each A/M bin: the colours refer to different values of the area-to-mass ratio; dashed lines indicate the result of the numerical propagation, solid lines the analytical one. It is possible to observe that the analytical model performs quite well in all the bins, even if its accuracy decreases for high A/M bins. This is due to the fact that high A/M bins correspond to a high mean eccentricity, so the hypothesis of circular orbits, required to write v_r as in Equation 13, introduces a certain level of error. The issues associated with this hypothesis are

discussed in the following section, but it is interesting to observe here that the dependency of mean eccentricity on the area-to-mass ratio is a product of how the velocity distribution is written in the NASA break up model.[23]

The number of fragments at the band formation is equal to 1826, which means that 24% of the fragments generated by the collision decay before the band formation. The analytical method predicts that after 1000 days, 1478 are still in orbit, against the result of 1405 obtained with the numerical integration: the relative error in the estimation of the fragment number is around 5%, so the analytical method can be considered a good approximation. During the 1000 days, the altitude of the density peak is reduced by 35% (Figure 8a); the peak location is basically unchanged (Figure 8b) for the cloud globally, whereas it undergoes a large variation for fragments with high area to mass ratio A/M. This is due to the fact, for the particular choice of the bin definition, the curves referring to high A/M values are more flat and the altitude corresponding to the peak (that is the point with the highest density) changes discontinuously.

Also the shape of the density function is affected by drag, which acts differently at low and high altitude. For this reason, the fragment density is reduced by 33% at an altitude smaller or equal to the parent altitude 800 km and only by 10% for higher altitudes. As the peak is reduced with time, the band of altitudes that contains 68.27%* of the population increases its amplitude with time (Figure 9).

Accuracy of the method

To estimate the accuracy of the method, the coefficient of determination R^2 is used,

$$R^2 = \frac{\sum_i (f_i - \bar{y})^2}{\sum_i (y_i - \bar{y})^2}, \tag{17}$$

that in statistics evaluates how the predictions of a model f_i fit the observed data y_i with average $\bar{y}$; R^2 close to 1 indicates that the model is able to represent the variation in the data. Here, the results of the numerical propagation are treated as the observed data and the analytical method is the model to be validated. The values of R^2 at four different times are shown in Table 1: R^2 is higher than 0.98 for the simulated time-span, so the analytical method shows a good agreement with the numerical data. In particular, the value of R^2 after 1000 days from the band formation is equal to 0.9848; using a single average value of A/M for the whole cloud would reduce this value to 0.9398.

Table 1: Coefficient of determination R^2 for the analytical method simulating a fragmentation at 800 km.

Days	R^2
0	1.000
333	0.989
666	0.988
1000	0.985

Computational time

Finally, it is interesting to compare the numerical and the analytical propagation also in terms of computational time, as shown in Figure 10: the intervals reported in the diagram refer to the case

*This percentage is borrowed from the definition of normal distribution, where 68.27% of the values lie within one standard deviation from the mean.

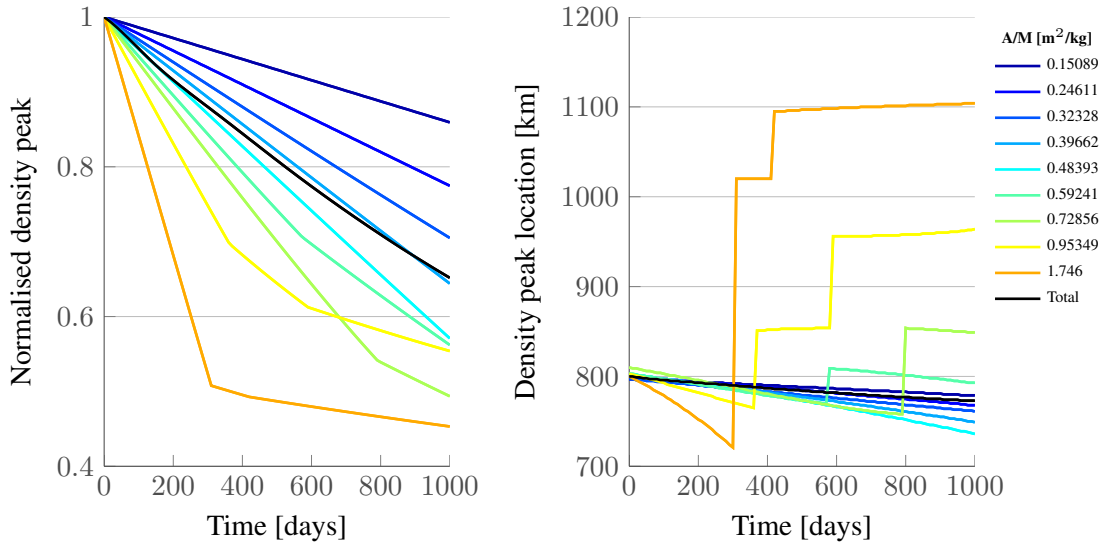

(a) Normalised peak height

(b) Peak location

Figure 8: Evolution of the density peak height and location for a fragmentation at 800 km. The value of the peak height is normalised with the value at band formation. The colours refer to different values of the area-to-mass ratio and in black the value for the cloud globally is reported.

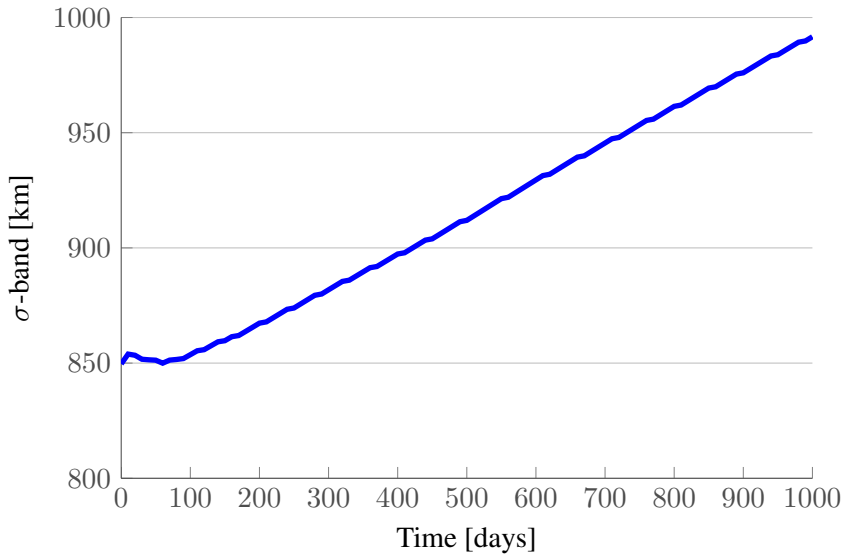

Figure 9: Evolution with time of the amplitude of the altitude band that contains 68.27% of the population for a fragmentation at 800 km.

shown in Figures 5-7, so the simulation of a cloud of initially 2397 fragments up to 1000 days after the band formation.

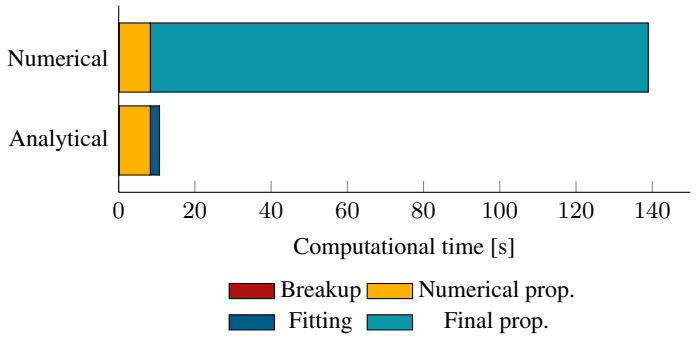

Figure 10: Computational time for a PC with 8 CPUs at 3.40 GHz.

The measured computational times refer to a PC with 8 CPUs at 3.40 GHz and the code for the numerical propagation is parallelised and written in Matlab. In both cases, the breakup model requires less than 0.1 s to generate the cloud. For the analytical method, the main contribution is given by the numerical propagation until the band formation (8.2 s), while the time for the final (analytical) propagation is negligible (0.027 s) and only 2.5 s are required to build the initial condition. On the other hand, the full numerical propagation takes 130 s to simulate 1000 days, as the simulation time for the numerical propagation depends on the number of fragments and the number of days. For this reason, the analytical approach is an efficient tool to simulate different collision scenarios.

Range of applicability

The method applicability was tested varying the initial orbit of the impacted spacecraft, both in inclination and in altitude.

Figure 11 shows the value of R^2 after 1000 days from the band formation for inclination ranging from 0 to 90 degrees: the value is always around 0.98, so the method follows correctly the cloud evolution for all the inclination values. The variation in R^2 is related to the fact that the ejection velocity direction is random and it was not kept constant for the different simulations.

Figure 12 shows the value of R^2 after 1000 days, but for different orbit altitudes: here R^2 is set equal to zero when it becomes negative as the meaning of null or negative values is that the model does not explain the observed data. This happens for low altitudes and, in general, the method seems to be applicable only for altitudes higher than 650 km. However, it should be observed that at high altitude (>800 km) also solar radiation pressure should be considered, while here it is neglected also in the full numerical case. The effect of solar radiation pressure and J_2 was investigated at higher altitudes[17] and a future work will focus on including it in the debris cloud analytical model, so in combination with drag.

Discussion on the effect of eccentricity

This section discusses the impact on the method accuracy of the assumptions made to obtain the analytical solution in Equation 15. Two hypotheses were introduced: the fragments are on circular orbits (Equation 13) and the distance of the fragments can be approximated with a fixed distance in part of the expression for the radial velocity (Equation 14). The contribution of each hypothesis

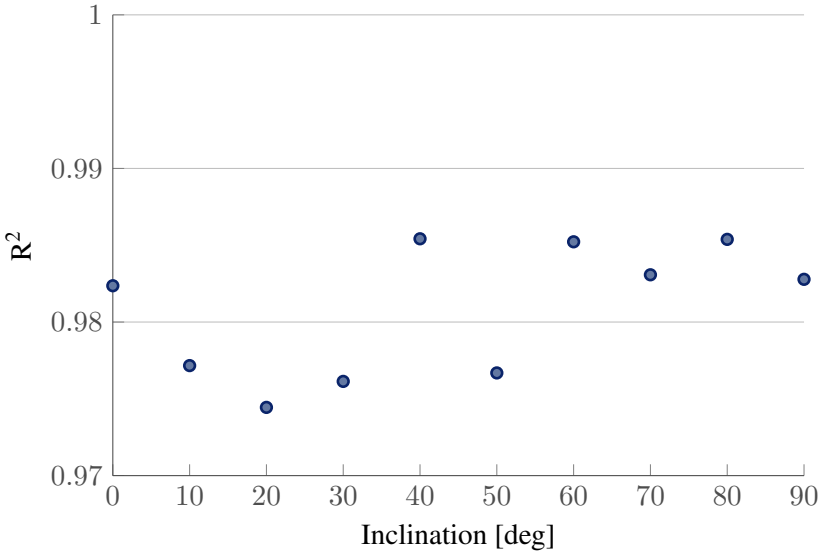

Figure 11: Accuracy of the method, measured by R^2 after 1000 days since the band formation, as a function of the inclination of the orbit where the fragmentation occurs (with fixed altitude equal to 800 km).

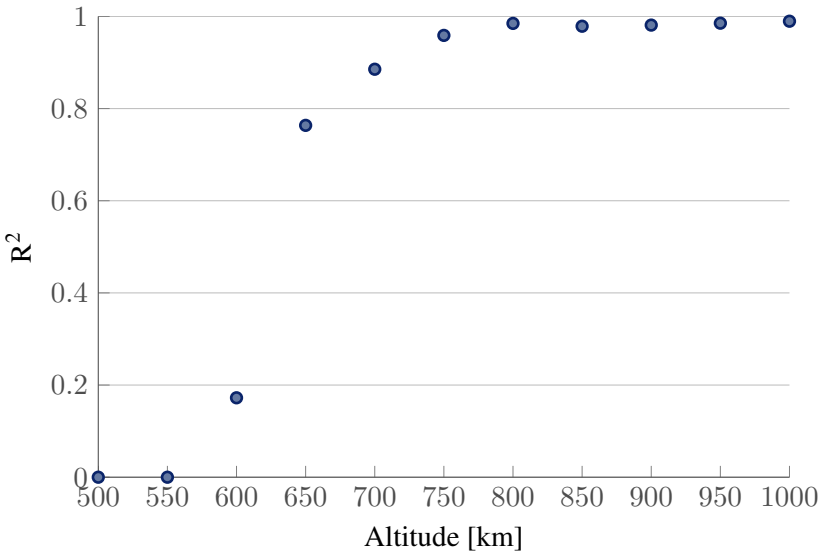

Figure 12: Accuracy of the method, measured by R^2 after 1000 days from the band formation, as a function of the fragmentation altitude.

is studied in Figure 13, where the variation in the semi-major axis after one period due to drag is plotted as a function of the semi-major axis. The plot is obtained considering that, starting from the altitude where the fragmentation occurs (in this case 500 km), it is possible to compute the maximum eccentricity that a fragment can have, given the semi-major axis of its orbit. In fact, all the fragments' orbits must include the point of fragmentation, which, in the two extreme cases, can be the apogee (Figure 13a) or the perigee (Figure 13b) of the fragment orbit. The maximum eccentricity is then the one associated with one of these two extreme cases: the fragmentation altitude is at the apogee for fragments with semi-major axis lower than the one of the parent orbit, whereas the fragmentation altitude is at the perigee for fragments with semi-major axis higher than the initial one. Knowing both the initial semi-major axis and the eccentricity, the decay of the fragment in one period can be computed. In Figure 13 the vertical lines indicate the eccentricity

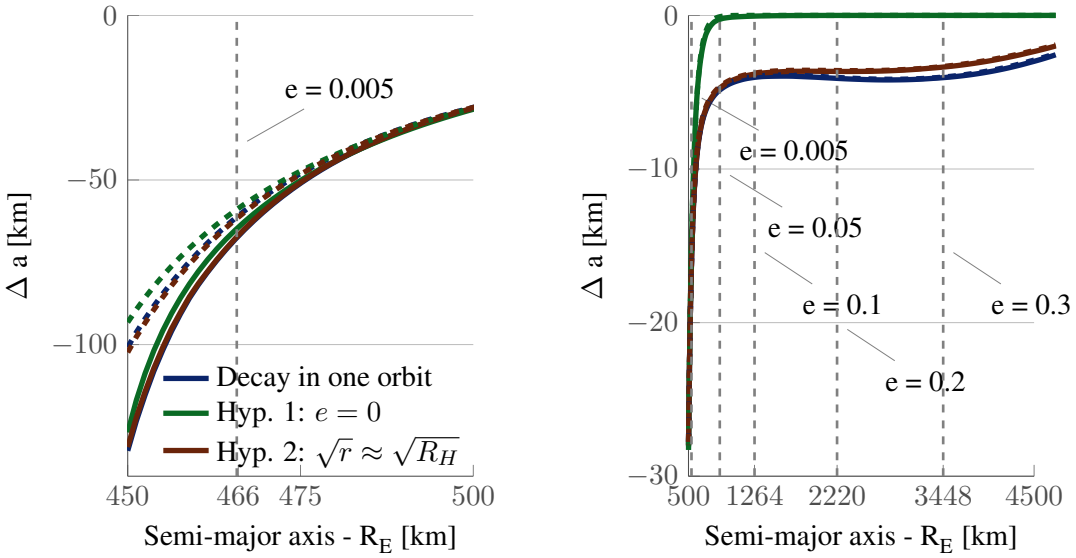

Figure 13: Variation of the semi-major axis in one orbit as a function of the orbit semi-major axis with different hypotheses for the integration, considering a fragmentation at 500 km. The vertical lines refer to eccentricity values.

The solid lines refers to the integration of the different models updating at each time step the parameters of the atmosphere and considering the actual value of the fragment altitude; the dashed line, instead, is obtained with the hypothesis that R_H, ρ_0, H are computed according to the fragmentation altitude and then kept constant for the whole simulation as explained in the method description.

The blue curve indicates the variation of the semi-major axis a obtained through numerical integration of Gauss' equations for a and the eccentricity e. The blue dashed line is, therefore, the reference curve that represents the results of the numerical propagation used to validate the analytical one.

The red curve is obtained through numerical integration of Gauss' equations for a and the eccentricity e, but assuming $\sqrt{r} \approx \sqrt{R_H}$: as shown in Figure 13, this hypothesis introduces a small but acceptable error.

The green curve represents the effect of the hypothesis $e = 0$ that is the integration only of

$$v_r = -\varepsilon\sqrt{a}\exp\Big(-\frac{a}{H}\Big) \tag{18}$$

and it is possible to observe that the fragment decay is underestimated, both at high and at low altitude. This is due to the fact that neglecting the eccentricity in the exponential term corresponds to applying an incorrect value of the density to compute the drag effect. In fact, using only the value of the semi-major axis, the information on the passage with low perigee, given by the eccentricity, is lost and the predicted decay is null.

For example, for a fragment with semi-major axis equal to $R_E + 1000\,\text{km}$ and corresponding eccentricity equal to 0.007, Gauss's equations estimate a reduction of the semi-major axis of $4.40\,\text{km}$ in 94 minutes. Introducing the approximation $\sqrt{r} \approx \sqrt{R_H}$, the predicted decay is $4.24\,\text{km}$, so the relative error is less than 4%. On the other end, with the hypothesis of circular orbit, the predicted decay is almost zero ($0.11\,\text{km}$) and so the effect of drag on the cloud is largely underestimated.

This effect is stronger at low altitude where a small variation in altitude results in a larger variation in density compared to what happens at higher altitude; in other words, at low altitudes the eccentricity value above which the decay is strongly underestimated is lower than at high altitude.

One could expect drag to affect the eccentricity distribution in such a way that the average eccentricity is reduced with time because of the progressive circularisation of the orbits. Actually, as shown in Figure 14, drag reduces the number of fragments, but especially those with low eccentricity as they also have low semi-major axis. The fragments with high eccentricity instead also have high energy and their decay is slow; their presence drives the average eccentricity to increase (for example, in the case in Figure 14 from 0.05 to 0.08). This means that the error due to eccentricity always increases with the simulation time.

Current work is aiming at including the eccentricity into the continuity equation, so that the method could be improved also at low altitudes. In this case, a full analytical formulation is not possible, in particular to express the characteristics of the new system. However, they can be expressed with known numerical functions that can be easily implemented and have a limited impact on the computational time.

CONCLUSIONS

Obtaining a reliable picture of the future debris environment requires the inclusion of small fragments ($< 10\,\text{cm}$) in long-term projections. Given the large number of fragments, simplified models have been studied to reduce the computational time required by simulations. In this work, an analytical method is proposed to obtain the evolution of a debris cloud generated by a collision.

The starting point for the method is the NASA breakup model, which provides the features of the fragments generated by a non-catastrophic collision; only the fragments whose size is between $1\,\text{mm}$ and $8\,\text{cm}$ were considered. The fragment orbital parameters were numerically propagated, accounting for the effect of atmospheric drag and the Earth's oblateness, until the distribution of the fragments could be considered spherically symmetrical and drag was the most relevant perturbation for fragment evolution. The information on fragment position was translated into a continuous function, using the fragment density probability along the orbit. Starting from the initial condition at the band formation, the evolution of the cloud density with time, under the effect of atmospheric drag, was obtained through the continuity equation. Under the hypothesis of circular orbits and con-

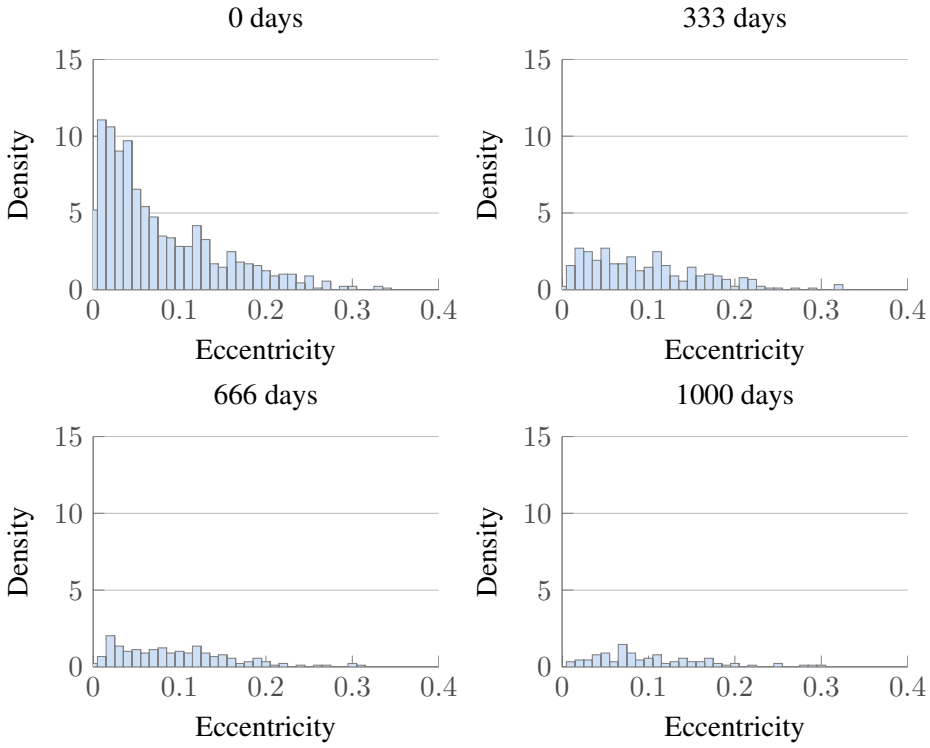

Figure 14: Evolution of the eccentricity distribution as a function of time, after the band formation, for a fragmentation at 500 km.

sidering an exponential model for the atmosphere, it was possible to derive an analytical expression for the fragment density as a function of time.

The method was validated through a comparison with the numerical propagation. For fragmentations occurring at altitudes higher than 650 km, the analytical method shows good accuracy for simulations up to 1000 days after the band closure, keeping the simulation time lower than 10% of the computational time of the numerical propagation. At lower altitudes, the hypothesis of circular orbits introduces a large error that suggests that eccentricity should be included in the analytical propagation. Future work will further develop the proposed method, as the present results suggest that the method may become an efficient tool to simulate a large array of collision scenarios. This can help to better understand the fragments' dynamics, to assess under which conditions a fragmentation event is more dangerous to operational satellites and to identify orbiting objects that, in case of fragmentation, are more likely to generate a debris cloud that can intersect other spacecraft and pose a hazard.

ACKNOWLEDGEMENT

The presentation of this paper was partially funded by the IET Travel Award. Francesca Letizia is also supported by the Amelia Earhart Fellowship for the academic year 2013/2014. The authors acknowledge the use of the IRIDIS High Performance Computing Facility, and associated support services at the University of Southampton, in the completion of this work.

REFERENCES

[1] R. Crowther, "Space Debris: mitigation and remediation," *Clean Space Workshop*, Harwell-Oxford Campus, October 2013.

[2] C. Wiedemann, C. Kebschull, S. K. Flegel, J. Gelhaus, M. Möckel, V. Braun, J. Radtke, I. Retat, B. Bischof, and P. Voersmann, "On-orbit fragmentation of Briz-M," *International Astronautical Congress*, Beijing, September 2013. IAC-13.A6.2.2.

[3] D. S. McKnight and F. Di Pentino, "Semi-Empirical Satellite Anomalies Analysis Highlighting Contributions from the Fengyun-1C Event," *International Astronautical Congress*, Beijing, September 2013. IAC-13.A6.2.1.

[4] P. H. Krisko, "The predicted growth of the low-Earth orbit space debris environment an assessment of future risk for spacecraft," *Proceedings of the Institution of Mechanical Engineers, Part G: Journal of Aerospace Engineering*, Vol. 221, Jan. 2007, pp. 975–985, 10.1243/09544100JAERO192.

[5] R. Walker, C. Martin, P. Stokes, and H. Klinkrad, "Sensitivity of long-term orbital debris environment evolution to the deployment of nano-satellite swarms," *Acta Astronautica*, Vol. 5, No. 1, 2002, pp. 439–449.

[6] C. Martin, R. Walker, and H. Klinkrad, "The sensitivity of the ESA DELTA model," *Advances in Space Research*, Vol. 34, Jan. 2004, pp. 969–974, 10.1016/j.asr.2003.02.028.

[7] A. E. White and H. G. Lewis, "The many futures of active debris removal," *Acta Astronautica*, Vol. 95, Feb. 2014, pp. 189–197, 10.1016/j.actaastro.2013.11.009.

[8] H. Krag, "Space Debris: techinical roadmap," *Clean Space Workshop*, Harwell-Oxford Campus, October 2013.

[9] A. Rossi, A. Cordelli, and C. Pardini, "Modelling the space debris evolution: Two new computer codes," *Advances in the Astronautical Sciences-Space Flight Mechanics*, 1995, pp. 1–15.

[10] D. King-Hele, *Satellite orbits in an atmosphere: theory and application*. Glasgow and London: Blackie, 1987.

[11] A. Cordelli, P. Farinella, and A. Rossi, "Study on Long Term Evolution of Earth Orbiting Debris," study note of work package 3200, ESA/ESOC Contract No. 10034/92/D/IM(SC), 1995.

[12] C. Kebschull, V. Braun, S. K. Flegel, J. Gelhaus, M. Möckel, J. Radtke, C. Wiedemann, H. Krag, I. Carnelli, and P. Voersmann, "A Simplified Approach to Analyze the Space Debris Evolution in the Low Earth Orbit," *International Astronautical Congress*, Beijing, September 2013. IAC-13.A6.2.3.

[13] J. Radtke, S. K. Flegel, V. Braun, C. Kebschull, C. Wiedemann, F. Schäfer, M. Rudolph, U. Johann, J. Utzmann, and M. Höss, "Fragmentation Consequence Analysis for LEO and GEO Orbits," *GreenOps Workshop*, Noordwijk, November 2013. ESA AO 1/7121/12/F/MOS.

[14] A. Rossi, G. B. Valsecchi, L. Anselmo, C. Pardini, H. G. Lewis, and C. Colombo, "Fragmentation Consequence Analysis for LEO and GEO Orbits," *GreenOps Workshop*, Noordwijk, November 2013. ESA AO 1/7121/12/F/MOS.

[15] C. R. McInnes, "An analytical model for the catastrophic production of orbital debris," *ESA Journal*, 1993.

[16] N. Gor'kavyi, "A new approach to dynamical evolution of interplanetary dust," *The Astrophysical Journal*, Vol. 474, No. 1, 1997, pp. 496–502.

[17] C. Colombo and C. R. McInnes, "Evolution of swarms of smart dust spacecraft," *New Trends in Astrodynamics and Applications VI*, New York, Courant Institute of Mathematical Sciences, June 2011.

[18] C. R. McInnes, "Simple analytic model of the long term evolution of nanosatellite constellations," *Journal of Guidance Control and Dynamics*, Vol. 23, No. 2, 2000, pp. 332–338.

[19] D. Izzo, *Statistical modelling of orbits and its application to trackable objects and to debris clouds*. PhD thesis, Università La Sapienza, 2002.

[20] S. Valk, A. Lemaître, and F. Deleflie, "Semi-analytical theory of mean orbital motion for geosynchronous space debris under gravitational influence," *Advances in Space Research*, Vol. 43, Apr. 2009, pp. 1070–1082, 10.1016/j.asr.2008.12.015.

[21] V. Chobotov, *Orbital mechanics*. Reston: American Institute of Aeronautics and Astronautic, 3rd ed., 2002.

[22] J.-C. Liou, "An active debris removal parametric study for LEO environment remediation," *Advances in Space Research*, Vol. 47, No. 11, 2011, pp. 1865 – 1876, http://dx.doi.org/10.1016/j.asr.2011.02.003.

[23] N. L. Johnson and P. H. Krisko, "NASA's new breakup model of EVOLVE 4.0," *Advances in Space Research*, Vol. 28, No. 9, 2001, pp. 1377–1384.

[24] P. H. Krisko, "Proper Implementation of the 1998 NASA Breakup Model," *Orbital Debris Quarterly News*, Vol. 15, No. 4, 2011, pp. 1–10.

[25] C. Pardini and L. Anselmo, "Review of past on-orbit collisions among cataloged objects and examination of the catastrophic fragmentation concept," *International Astronautical Congress*, Beijing, September 2013. IAC-13.A6.2.9.

[26] F. Schäfer, M. Rudolph, and U. Johann, "Fragmentation Consequence Analysis for LEO and GEO Orbits," *GreenOps Progress Meeting*, Noordwijk, November 2013. ESA AO 1/7121/12/F/MOS.

[27] F. Schäfer, M. Quarti, M. Roll, P. Matura, M. Rudolph, R. Putzar, M. Reichel, J. Hupfer, and K. Buehler, "Fragmentation studies of simple cubic structures at Fraunhofer EMI," *Sixth European Conference on Space Debris*, Darmstadt, April 2013.

[28] J. C. Liou, N. Fitz-Coy, S. Clark, M. Werremeyer, T. Huynh, M. Sorge, M. Voelker, and O. J., "DebriSat - A planned laboratory based satellite impact experiment for breakup fragment characterization," *Sixth European Conference on Space Debris*, Darmstadt, April 2013.

[29] H. Sdunnus, P. Beltrami, H. Klinkrad, M. Matney, A. Nazarenko, and P. Wegener, "Comparison of debris flux models," *Advances in Space Research*, Vol. 34, Jan. 2004, pp. 1000–1005, 10.1016/j.asr.2003.11.010.

[30] R. Jehn, "Dispersion of debris clouds from In-orbit fragmentation events," *ESA Journal*, Vol. 15, No. 1, 1991, pp. 63–77.

[31] D. A. Vallado, *Fundamentals of astrodynamics and applications*. Springer, 2001.

[32] J. E. Gentle, *Elements of computational statistics*. Springer, 2002.

[33] V. Chobotov, "Dynamics of orbiting debris clouds and the resulting collision hazard to spacecraft," *JBIS. Journal of the British Interplanetary Society*, 1990.

[34] D. S. McKnight, "A phased approach to collision hazard analysis," *Advances in Space Research*, Vol. 10, Jan. 1990, pp. 385–388, 10.1016/0273-1177(90)90374-9.

[35] J. Ashenberg, "Formulas for the phase characteristics in the problem of low-Earth-orbital debris," *Journal of Spacecraft and Rockets*, Vol. 31, Nov. 1994, pp. 1044–1049, 10.2514/3.26556.

[36] F. Letizia, C. Colombo, H. G. Lewis, and C. R. McInnes, "Debris cloud evolution in Low Earth Orbit," *International Astronautical Congress*, Beijing, September 2013. IAC-13.A6.P.12.

[37] C. R. McInnes and C. Colombo, "Wave-like patterns in an elliptical satellite ring," *Journal of Guidance, Control, and Dynamics*, 2013.